Accepted Manuscript

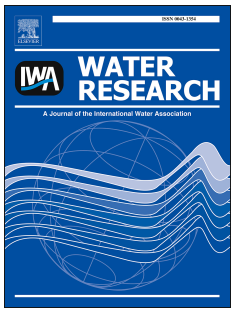

Elucidating the impacts of initial supersaturation and seed crystal loading on struvite precipitation kinetics, fines production, and crystal growth

Shantanu Agrawal, Jeremy S. Guest, Roland D. Cusick

PII: S0043-1354(18)30002-2

DOI: 10.1016/j.watres.2018.01.002

Reference: WR 13481

To appear in: *Water Research*

Received Date: 28 August 2017

Revised Date: 15 December 2017

Accepted Date: 1 January 2018

Please cite this article as: Agrawal, S., Guest, J.S., Cusick, R.D., Elucidating the impacts of initial supersaturation and seed crystal loading on struvite precipitation kinetics, fines production, and crystal growth, *Water Research* (2018), doi: 10.1016/j.watres.2018.01.002.

Graphical Abstract

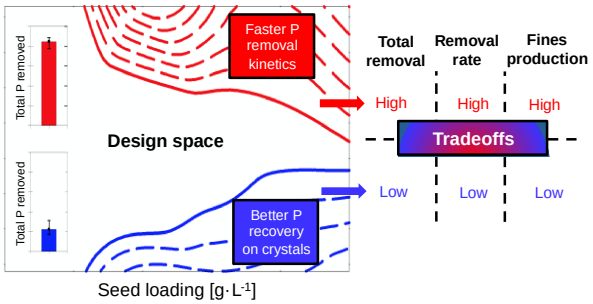

Elucidating the impacts of initial supersaturation and seed crystal loading on struvite precipitation kinetics, fines production, and crystal growth

Shantanu Agrawal[1,2], Jeremy S. Guest[1], Roland D. Cusick[1]*

[1]Department of Civil and Environmental Engineering, University of Illinois at Urbana-Champaign, 205 North Mathews Avenue, 3217 Newmark Civil Engineering Laboratory, Urbana, Illinois 61801, USA

*Corresponding author contact information:

Roland D. Cusick, Ph.D.

Department of Civil & Environmental Engineering

University of Illinois at Urbana-Champaign

3217 Newmark Civil Engineering Laboratory, MC-250

205 North Mathews Avenue

Urbana, IL 61801-2352

Phone: (217) 244-6727

E-Mail: rcusick@illinois.edu

[2] Present Address: Carollo Engineers, Inc. 8600 W Bryn Mawr Ave, Suite 900N, Chicago, Illinois 60631, USA.

Key words

Struvite Precipitation, Nucleation, Phosphorus, Nutrient Recovery, Wastewater Treatment

Abstract

To reduce intra-plant nutrient cycling and recover phosphorus (P) fertilizers from nutrient-rich sidestreams, wastewater utilities increasingly elect to employ struvite precipitation processes without a clear understanding of the inherent tradeoffs associated with specific design and operating decisions. Specifically, the impact of reactor conditions on struvite crystallization rate and distribution between formation of fines particles and secondary growth onto large diameter seed crystals represent critical knowledge gaps limiting the predictive capabilities of existing process models. In this work, the relative impacts of initial supersaturation (S_i) and seed loading on P removal kinetics and struvite solids distribution were investigated. In experiments conducted at different levels of initial supersaturation (1.7 – 2.4) and seed loading (0 – 25 g L^{-1}), struvite fines represented the majority of phosphate solids formed in 10 of 12 conditions. While total P removal was dependent on S_i, and primarily attributed to formation of fines, the concentration of struvite seed granules had a significant impact on the rate of P removal. Struvite seed granules increased the rate of precipitation by reducing induction time of primary nucleation of struvite fines. Secondary crystal growth represented the majority of struvite solids formed at high seed loading and low S_i, but presented the tradeoff of low total removal and low rate of removal. To convey the significance of these findings on process modeling, we show how a prominent kinetic model with a first order dependency on solid struvite concentration over-predicts P removal rate when total mass is dominated by large diameter seeds (0.9 mm). This works reveals the critical role of struvite fines in P removal and highlights the need to account for their production and kinetic importance in struvite process design and operation.

1. Introduction

The phosphorus (P) contained in human excreta presents sanitation utilities with both an operational challenge and opportunity to contribute to the sustainable management of one of society's most essential resources. To reduce the contribution of point-source nutrient discharge to major U.S. coastal hypoxic zones, such as the Gulf of Mexico and Chesapeake Bay, water resource recovery facilities (WRRFs; a.k.a. wastewater treatment plants, WWTPs) are facing increasingly stringent regulations of P in treated effluent. As of 2016, 23 states in the U.S. already had some level of EPA-approved numeric total P criteria for different water types (US EPA, 2016). As WRRFs adapt to meet these emerging water quality regulations, facilities could also help displace mined fertilizers if soluble P removal is accompanied with recovery. It is estimated that 22% of the total global P demand in 2009 could have potentially been satisfied through the P available in human urine and feces (Mihelcic et al., 2011). If the influent wastewater contains sufficient carbon, implementing Enhanced Biological Phosphorus Removal (EBPR) can enable effluent P concentrations below most discharge limits (0.1 - 1 $mg \cdot L^{-1}$) (Burn et al., 2014; Clark et al., 2010; Parsons and Smith, 2008). However, luxury P uptake by polyphosphate accumulating organisms (PAOs, up to 20-30% of their dry weight as P) in the aerobic zone of EBPR is released in the absence of aeration during sludge handling, which increases intra-plant nutrient cycling and can lead to P-mineral scale formation on sidestream conveyance conduit and equipment (Münch and Barr, 2001; Parsons and Smith, 2008; Woods et al., 1999).

Controlling phosphate mineral formation within crystallization reactors is gaining momentum as an efficient means of reducing nutrient cycling and scaling potential, while also offsetting operating costs through the sale of recovered fertilizer. To fully realize plant specific benefits associated with sidestream P removal, precipitation reactors must be designed and operated to not only convert soluble P to struvite but also collect all of the solids that form. Unlike calcium

phosphate minerals, which forms in wastewater as difficult to capture amorphous phase particles (Seckler et al., 1996), magnesium ammonium phosphate hexahydrate ($MgNH_4PO_4 \cdot 6H_2O$; struvite) forms large diameter crystals (via heterogeneous nucleation or secondary growth) with high average settling velocity (Britton et al., 2005; Jaffer et al., 2002; Muster et al., 2013; Wang et al., 2005), enabling both treatment and recovery. Most struvite recovery processes operate with high seed crystal loadings to enhance secondary growth onto seed surfaces, but distribution of growth between struvite seed crystals and new colloidal struvite fines remains poorly understood. With an increase in extractive nutrient recovery installations (Latimer et al., 2016), utilities are making substantial investments in sidestream P recovery processes without a clear understanding of the true benefits of different designs and operating strategies. Although current full-scale struvite recovery systems (e.g., Ostara Pearl™, NuReSys, Phosnix, and PHOSPAQ™) all advertise high soluble phosphate removal efficiency (80 - 90%) and similarly broad P handling capacities (60 - 900 mg PO_4-P/L), the impacts of reactor design (fluidized bed reactors vs. completely stirred tank reactors) and operating pH (which increases precipitation driving force, i.e., supersaturation) on solids recovery and product quality remain unclear (Desmidt et al., 2015; Ye et al., 2017). If struvite fines represent a significant fraction of solids formed during treatment, measuring process efficiency in terms of soluble phosphate removal could be misleading since fine particles can easily washout and re-dissolve in downstream processes (Baur et al., 2008; Crutchik et al., 2017; Grooms et al., 2015). Excess production and loss of struvite fines from precipitation reactors can also affect the validity of modeling assumptions and economic predictions for struvite crystal recovery and reuse.

As evidenced by the multitude of models for struvite crystallization that exist in the literature, the research community has yet to reach consensus on a kinetic process model that accurately and efficiently predicts both soluble phosphate removal and the distribution of crystallite growth

between seeds and fines. Struvite crystallization rate has been defined using several approaches: power law correlation with relative supersaturation (Kofina and Koutsoukos, 2005; Rahaman et al., 2014); dependence on crystals mass ratio, specific surface area of crystals, and relative supersaturation (Mehta and Batstone, 2013). While some have neglected or lumped the nucleation and aggregation kinetics into crystal growth rate expressions (Mehta and Batstone, 2013; Rahaman et al., 2014), others have individually characterized the kinetics of nucleation, crystal growth, and aggregation using a dynamic particle population mass balance (Galbraith et al., 2014; Lizarralde et al., 2015). Coupling soluble P removal to particle size and surface area dynamics, while intuitive, introduces the need for a particle counting device with a broad detection limit and several fitting parameters that cannot be externally calibrated, both of which limit the applicability of these approaches at full-scale. Recently, a computationally lean modeling approach with a first order dependence on struvite concentration and relative supersaturation (Kazadi Mbamba et al., 2015b) was recently integrated with a plant-wide model to project the significant benefits of sidestream struvite total nutrient removal capacity and plant effluent P concentration (Kazadi Mbamba et al., 2016). To evaluate if this approach has merit for full-scale struvite recovery systems, the model must be validated with struvite seed loadings and particle diameters that reflect full-scale operation.

The objective of this work was to investigate the influence of solution supersaturation and seed crystal loading on struvite solids distribution (i.e., fines versus secondary crystal growth) and precipitation kinetics. Batch experiments were conducted using synthetic wastewater containing struvite-forming ions at concentrations typical of anaerobic digester supernatant and sludge centrate, at multiple levels of seed loading and initial supersaturation (S_i) with respect to struvite. Experimental results were used to explore and understand potential tradeoffs between removal and recovery in struvite precipitation processes. Experimental data were also used to

100 better understand the efficacy and validity of current modeling techniques, and identify a path
101 forward for model development and process design.

102 **2. Materials and methods**

103 Experiments were designed to create an initial driving force for precipitation
104 (supersaturation, eq. 3) and measure the amount of struvite that forms onto existing seed
105 crystals (struvite granules collected from a full-scale crystallization reactor), or through the
106 production of fine particles, as the system approaches equilibrium. As described below (section
107 2.4) chemical base was excluded from all experiments to reduce the impacts of localized
108 supersaturation on fines production due to incomplete mixing. All experiments were conducted
109 at room temperature (21 – 23 °C) in 1 L beakers, and a mixing speed of 300 rpm was used to
110 be consistent with other nucleation studies (Mehta and Batstone, 2013; Ohlinger et al., 1999).
111 Experimental data were used to quantify reaction kinetics of struvite formation (section 2.5) and
112 evaluate the validity of a prominent precipitation process model under high seed loading
113 (section 2.6). For all experiments, initial chemical concentrations of the synthetic solutions were
114 2.2 mM of PO_4^{3-}, 2.6 mM of Mg^{2+}, and 50 mM of NH_4^+. Given that ammonium was in excess for
115 all experimental conditions, a Mg to P ratio of 1.2:1 was chosen to maximize the purity of
116 struvite precipitation (Muster et al., 2013). The P concentration used was typical of centrate or
117 filtrate for post-anaerobic digestion and in range of the P concentrations entering full-scale
118 struvite recovery processes (Battistoni et al., 1998; Desmidt et al., 2015). Solution composition
119 excluded impurities that would impact precipitate phase and product size (e.g., calcium and
120 carbonate ions, dissolved organic matter, and inert particulates) in order to quantify the impact
121 of supersaturation and seed loading on struvite mass distribution and modeling accuracy.

122 *2.1. Solution preparation*

123 Experimental solutions were prepared by mixing aliquots of ammonium chloride and
124 magnesium chloride with a sodium phosphate solution composed of specific quantities of mono-

, di-, and tribasic sodium phosphate to obtain a specific initial thermodynamic driving force for precipitation. Initial chemical concentrations of the synthetic solutions were approximately maintained at 2.2 mM of total phosphate, 2.64 mM of total magnesium, and 50 mM of total ammonia, while supersaturation was adjusted with pH. The ammonium concentration in solution was significantly higher than phosphate and magnesium to reflect $Mg:NH_4:PO_4$ ratios observed in wastewater and to promote formation of struvite over newberyite and amorphous magnesium phosphate (Abbona et al., 1982, 1984; Abbona and Boistelle, 1979; Crutchik and Garrido, 2011). All stocks solutions were prepared by dissolving ACS grade inorganic salts (NH_4Cl, $MgCl_2 \cdot 6H_2O$ $NaH_2PO_4 \cdot H_2O$, Na_2HPO_4, and $Na_3PO_4 \cdot 12H_2O$; Sigma-Aldrich, MO, USA) in distilled water (ASTM Type II). Stock solutions were well-mixed using magnetic stirrers and were diluted with distilled water to the target concentrations before use.

2.2. Analytical Methods

Solution pH was continuously monitored to quantify induction of precipitation and ionic speciation with time for each experiment (Orion VERSA STAR; Thermo Scientific, MA, USA). Total dissolved phosphorous was measured using the Molybdovanadate Method with Acid Persulfate Digestion Test 'N Tube™ Procedure (Hach, CO, USA) after filtering samples through 0.22 μm (Durapore 0.22 μm PVDF Membrane Filter, item no. GVWP02500; EMD Millipore, MA, USA). The turbidity of the solutions, which was used as a qualitative indicator of fines production, was monitored using a Hach 2100Q Turbidimeter (Hach, CO, USA). Solution turbidity measurements have been shown to correlate with the formation of struvite particles ranging from 5 – 120 μm (Triger et al., 2012).

2.3. Induction Time Study

Experiments were conducted to characterize the induction time of homogeneous nucleation (no seed granules) in solutions at different levels of supersaturation, with and without the addition of sodium hydroxide (NaOH). Although NaOH is commonly used for pH adjustment

in nucleation studies, it was hypothesized that its addition would expedite nucleation by generating localized zones of high pH as the concentrated base is mixed into solution. To test this hypothesis, ten solutions were prepared with identical concentrations of total phosphate, total magnesium, and total ammonium. Five levels of supersaturation (from 1.8 to 2.6) were achieved in duplicate by adjusting pH, either (i) through NaOH (1 N) addition or (ii) by selecting different combinations of dibasic and tribasic sodium phosphate. Induction time has been shown to be primarily dependent on supersaturation (Bhuiyan et al., 2008; Mehta and Batstone, 2013; Ohlinger et al., 1999) using the expression:

$$\log t_{ind} = \frac{A}{(\log S)^2} - B \quad (1)$$

where t_{ind} (sec) is the measured induction time, S is supersaturation, and A and B are empirical constants. Induction time was defined as the time taken for the pH to decrease by 0.05 below its initial value in a batch reactor, as previously described (Mehta and Batstone, 2013). Solution pH can be used as an indicator for precipitation since struvite formation at near neutral pH involves HPO_4^{2-} and produces an equivalent of acid per mole of struvite formed:

$$NH_4^+ + Mg^{2+} + HPO_4^{2-} \leftrightarrow NH_4MgPO_{4(s)} + H^+ \quad (2)$$

Preliminary unseeded precipitation experiments indicated the induction time of nucleation was sensitive to the addition of NaOH at lower values of supersaturation (Fig. S1). Since induction time is inversely related to supersaturation, increased rate of fines production associated with NaOH (Fig. 1) may be attributed to the formation of localized zones of higher supersaturation when base was added to adjust initial pH. To avoid the bias of enhanced fines production in subsequent experiments, the kinetics of phosphate removal were further studied by allowing solutions to reach equilibrium without any addition of NaOH (neither for initial pH adjustment or pH control).

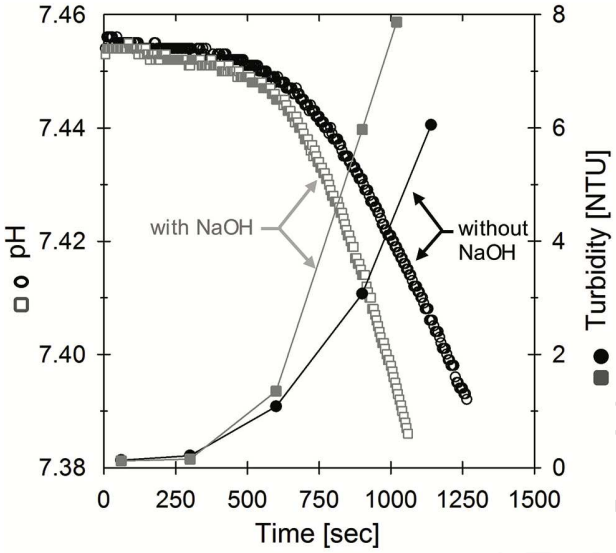

Fig. 1. Variation of pH (primary y-axis) and solution turbidity (secondary y-axis) with time for experimental solutions prepared with and without NaOH at an initial supersaturation of 1.8. The rate of pH decrease and turbidity increase (attribute to fines formation) was higher when NaOH was used to prepare the solution. Since the addition of NaOH promoted fines production, all solutions for kinetic experiment were thus prepared without NaOH.

2.4. Kinetic Experiments

Batch experiments were conducted to understand the impacts of seed loading and supersaturation on kinetics of phosphate removal and struvite production as fines. Experiments were conducted in duplicate at initial superstations (S_i) of 1.7, 2.1, and 2.4 across all seed loadings of 0 $g \cdot L^{-1}$, 5 $g \cdot L^{-1}$, 15 $g \cdot L^{-1}$, and 25 $g \cdot L^{-1}$. Struvite seeds used in this study were 0.9 mm (90 SGN) in diameter and were provided by Ostara (Vancouver, Canada). These saturation values are intentionally low to promote secondary growth onto existing seeds. To avoid spatial and temporal gradients in supersaturation from chemical addition that could promote nucleation (described in 2.3), experimental solutions were allowed to reach equilibrium without maintaining a fixed level of supersaturation. Kinetic experiments were run for 3 hours (during which time all solutions reached equilibrium) and were sampled at different time points for phosphate and turbidity readings. At the end of the experiments, struvite granules were dried in an oven at

40°C for 48 hours to prevent any loss of water of crystallization from the struvite crystals (Ohlinger et al., 1999). To determine the amount of struvite solids that precipitated onto the seeds, the granules were weighed before and after each experiment. The mass of fines generated in each experiment were defined as the molar difference between soluble P removal and seed growth.

2.5. Calculations

Experimental data collected in batch precipitation experiments were used to estimate struvite supersaturation as a function of time and second order kinetic rate constants for struvite precipitation (hr^{-1}). The struvite precipitation potential (or supersaturation, S) for any solution was defined by:

$$S = \left(\frac{\{Mg^{2+}\}\{NH_4^+\}\{PO_4^{3-}\}}{K_{sp}}\right)^{1/3} \quad (3)$$

where {} represents the activity of an ion and K_{sp} is the thermodynamic solubility product. The value of K_{sp} used in this work was 5.49×10^{-14} (pK_{sp} = 13.26) (Mehta and Batstone, 2013; Ohlinger et al., 1998).

The values of equilibrium constants and heat enthalpies for dissociation of the different species considered were taken from literature (Bhuiyan et al., 2007; Rahaman et al., 2006). The Van't Hoff equation was used to correct the values of equilibrium constants for temperature variations and Davies equation was used to find the activity coefficient of different species in the solution. Since struvite was the only supersaturated mineral under all experimental conditions (Table S1), the decrease in molar concentrations of Mg^{2+} and NH_4^+ was assumed to be equal to the corresponding decrease in PO_4^{3-} molar concentrations. MATLAB (R2015a; MathWorks®, USA) was used to calculate the value of supersaturation and solve for the concentration of each ionic species at time points for the duration of the experiment. The interactions of the different ionic species and compounds considered in this study were (Rahaman et al., 2014): Mg^{2+}, NH_4^+,

PO_4^{3-}, $MgNH_4PO_4 \cdot 6H_2O_{(s)}$, $H_3PO_{4(aq)}$, $H_2PO_4^-$, HPO_4^{2-}, $MgH_2PO_4^+$, $MgHPO_{4(aq)}$, $MgPO_4^-$, $MgOH^+$, $NH_{3(aq)}$, H^+, and OH^-.

The values of the kinetic rate constant for P removal were derived using regression analysis between relative supersaturation and time (Fig. S3). A pseudo-2nd order relationship with respect to relative supersaturation was used as the aqueous concentration of ammonium (NH_4^+) was in excess relative to phosphate (PO_4^{3-}) and magnesium (Mg^{2+}). Experimental data prior to reaching a steady state were used to determine the kinetic parameters as the solution reached equilibrium (Nelson et al., 2003). The r-squared values of the fits for the pseudo-2nd order kinetics plots were greater than 0.90 except for one, which was 0.87.

2.6. Modeling Analysis

Crystal growth modeling is critical to process development and system optimization as it allows us to traverse the design and operational landscape. Recently, a mineral precipitation approach for struvite using Eqn. (4) was used while modeling a multi-species system with multiple mineral precipitation processes (Kazadi Mbamba et al., 2015b, 2015a). Based on this kinetic modeling approach, plant-wide models for tracking P transformations and evaluating struvite precipitation in wastewater treatment systems are being built (Kazadi Mbamba et al., 2016; Solon et al., 2017). We leveraged our experimental data to evaluate the validity of a prominent kinetic model (Eq. 4) (Kazadi Mbamba et al., 2015b, 2015a) to understand the efficacy of this approach in predicting soluble P removal and struvite formation at high seed loadings. The evaluated rate expression is as follow:

$$r_{cryst} = k_{cryst} X_{cryst} \sigma^n \quad (4)$$

where r_{cryst} is the mineral precipitation rate (moles$\cdot L^{-1} \cdot h^{-1}$), k_{cryst} is the kinetic rate constant (h^{-1}), X_{cryst} is the concentration of precipitate at any time (moles$\cdot L^{-1}$), σ is relative supersaturation (σ = S -1) and n is the order of the reaction. This modeling approach for mineral precipitation rate has not been assessed in the presence of larger size struvite particles, which are typically

present in large full-scale struvite reactors. Supersaturation values from the experimental data were used to predict the mineral precipitation rate of struvite and were then compared with the actual observed mineral precipitation rate of struvite to calculate the residuals (the difference between the observed rate and predicted rate). The value of n was taken to be 3 and the value of k_{cryst} for struvite was assumed to be 3.2 h^{-1}, as found for synthetic wastewater (Kazadi Mbamba et al., 2015b). The value of X_{cryst} was assumed to be constant throughout the length of all batch experiments since the concentrations of struvite that precipitated in the experiments were negligible as compared to the concentrations of the struvite seed crystals (< 4.1%).

3. Results and discussion

3.1. P removal and struvite solids distribution

The extent of soluble P removal in batch experiments was dependent on initial supersaturation (S_i), while the distribution of struvite production was dependent on both S_i and seed loading. Total solution phosphate removal ranged from 0.22 ± 0.04 mM at the lowest initial supersaturation (S_i = 1.7) to 0.84 ± 0.03 mM at the highest (S_i = 2.4), starting from an initial phosphate concentration of 2.2 mM as PO_4^{3-} in all batch experiments (Fig. 2, Left). As described in section 2.4, experimental solutions were allowed to approach equilibrium without maintaining a fixed level of supersaturation (average final across all experiments S = 1.2 ± 0.02). As a result, total P removal was comparatively lower (10 - 38%) than values observed for full scale processes (80 - 90%) (Desmidt et al., 2015) in which chemicals are added (NaOH and $MgCl_2$) to maintain a constant level of supersaturation. Fines represented the majority of struvite solids formed in all but two experimental conditions (S_i = 1.7 at 15 $g \cdot L^{-1}$ and 25 $g \cdot L^{-1}$) (Fig. 2). While the percentage of struvite solids attributed to secondary growth of seed crystals increased with seed loading for each value of S_i, observed increases in P removal was primarily attributed to the production of new particles (Fig. 2, Right). High seed loading can be used to exert control

265 over secondary crystal growth (Fig. 2A, Right), but supersaturation must be kept low to minimize
266 fines production.

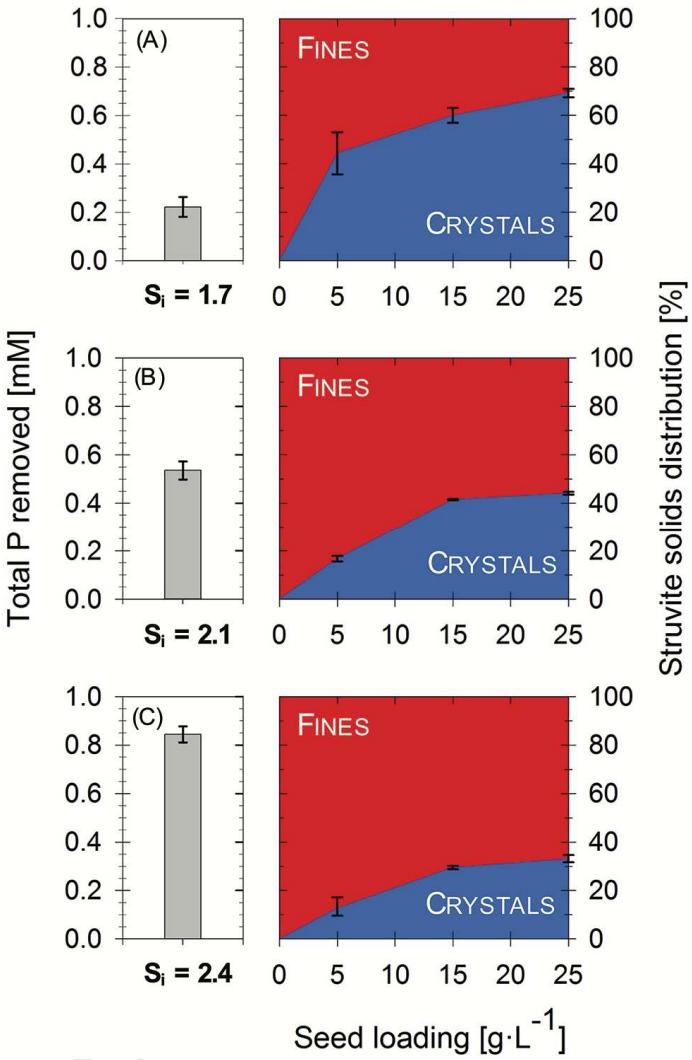

267
268 **Fig. 2.** (Left) Total phosphate removal averaged across all the seed loadings (0 g·L^{-1}, 5 g·L^{-1}, 15 g·L^{-1},
269 and 25 g·L^{-1}) for a particular value of initial supersaturation (S_i): (A) S_i = 1.7; (B) S_i = 2.1; (C) S_i = 2.4.
270 Error bars represent the standard deviations for the averaged removals across all seed loadings.
271 (Right) Distribution of struvite precipitation onto seed crystals (blue colored region) or as fines (red
272 colored region) for each seed loading and corresponding value of initial supersaturation (S_i). Error
273 bars represent the minimum and maximum values of the experimental replicates. As solutions
274 reached equilibrium, the total P removed was independent of seed loading and increased with S_i.

Fines represented the majority of struvite solids formed across different seed loading concentrations and S_i for 10 of the 12 experiments.

3.2. Effects of seed loading and initial supersaturation on kinetics and fines production

The percentage of total phosphate removal associated with struvite fines was dependent on both seed loading and initial supersaturation (Fig. 3A). Higher seed loadings and lower values of initial supersaturation maximized secondary crystal growth on struvite seeds while minimizing the production of suspended struvite fines in the solution. Higher recoveries of the struvite formed via secondary crystal growth on the seed crystals were observed at the cost of lower soluble phosphate removal (Fig.2, Left) due to slower removal kinetics (Fig. 3B). For example, the highest recovery of the struvite formed via secondary crystal growth on the seed crystals was 69.31% ($\pm$ 1.75) at a seed loading of 25 $g \cdot L^{-1}$ and initial supersaturation (S_i) of 1.7 (Fig. 2 Right). But the total phosphate removed at this condition was only 0.2 mM (Fig. 2 Left).

The kinetic rate of phosphate removal via struvite precipitation also exhibited dependence on both seed loading and initial supersaturation (Fig. 3B). The kinetic rate constant appeared to plateau as seed loading was increased at higher values of initial supersaturation (S_i = 2.4) (Figs. S5 and S2). At these conditions, kinetics of P removal was governed by fines production instead of secondary crystal growth (Fig. 2C). The greatest shift in the kinetic precipitation rate was observed during the transition from no seeds to a seed loading of 5 $g \cdot L^{-1}$ at the higher initial supersaturation (S_i > 2.1), and can be attributed to an observed decrease in the total induction time (Fig. 4A). The change in seed loading concentration from 0 $g \cdot L^{-1}$ to 5 $g \cdot L^{-1}$ at S_i of 1.7 eliminated the precipitation lag-phase that was observed in the absence of seed crystals (Fig. 4B). These results indicate that the designation of metastability for primary nucleation are not applicable in the presence of seed crystals (Fig. 4B). Total induction time also showed a waning dependence on both seed loading and initial supersaturation (Fig. 4A). These findings elucidate a potential important design and operation trade-off. Systems designed to

optimize struvite recovery at higher seed loadings and lower initial supersaturations may require longer residence times than those that promote rapid removal through heterogeneous nucleation of fines.

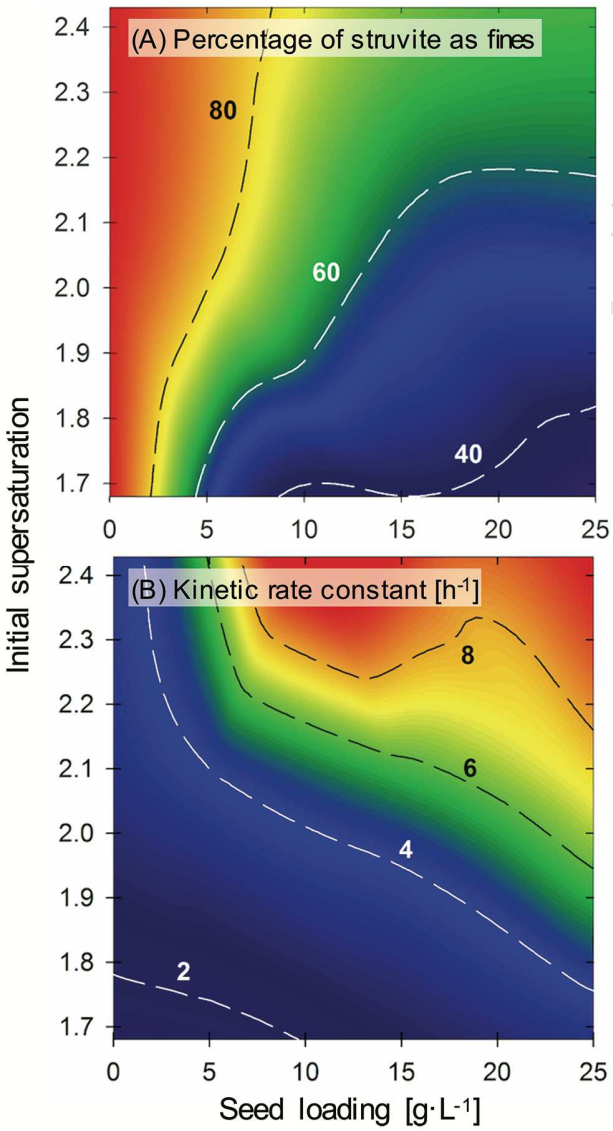

Fig. 3. The observed effect of seed loading (x-axis) and initial supersaturation (y-axis) on (A) the percentage removal of total phosphate associated with the formation of struvite fines, and (B) the variation of the kinetic rate constant for phosphate removal. The highest percentage of fines aligned with the highest rate of removal. Raw data for figure can be found in Table S2 and Table S3.

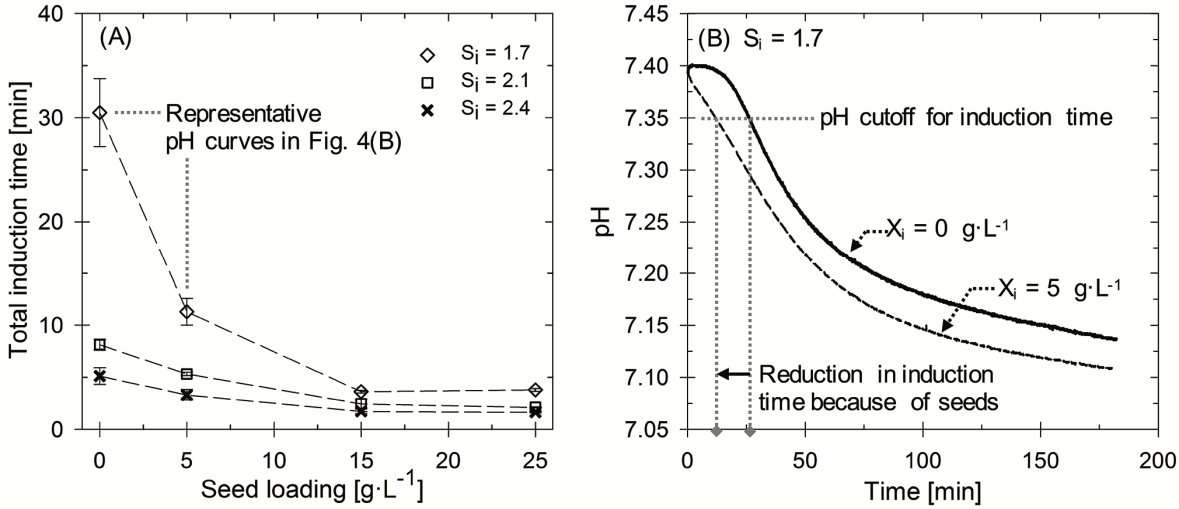

Fig. 4. (A) Total Induction time at various seed loading concentrations for different levels of initial supersaturation. Error bars represent the minimum and maximum values of the experimental replicates. (B) pH profiles for seed loading concentrations of 0 $g \cdot L^{-1}$ and 5 $g \cdot L^{-1}$ at the same level of initial supersaturation (S_i = 1.7). pH was used to characterize induction time and track the kinetics of struvite precipitation.

3.3. Engineering Design Implications

Assuming our results translate to full-scale reactors, recovery of fines will broadly dictate the struvite collection efficiency of a process. Ostara Pearl™ upflow fluidized bed reactors, which represent the majority of operational full-scale struvite recovery systems, work at conditions of high seed loading and lower values of supersaturation (characterized by target pH values as low as 6.9 and 7.2) (Baur et al., 2008; Britton et al., 2009), thus maximizing the collection efficiency. But if struvite fines are produced, the potential for process disruption could increase because of the associated risks with fines washout from the high recycle rate of fluidized bed reactors. Since the kinetics of P removal and production of fines were most sensitive to saturation at high seed loading (Fig. 3A and B), addition of magnesium and base to maintain saturation likely creates spatial and temporal variations in precipitation rate and mechanism. Struvite precipitation in the NuReSys process occurs at a higher pH range of 8-8.5

and supersaturation (assuming similar concentrations) (Desmidt et al., 2015; Ye et al., 2017), indicating that both fines production and removal kinetics may be higher in this system. Despite this difference, NuReSys systems achieve similar removal (80 – 90%) and produce struvite particles in the range of 1-3 mm (Desmidt et al., 2015; Moerman, 2011) which is similar to values reported for Ostara Pearl^{TM} FBRs (1-4.5 mm) (Desmidt et al., 2015; Grooms et al., 2015). Since the NuReSys system promotes formation and capture (with a hydrocyclone), the risk of washout may be lower than fluidized bed systems. Most importantly, recovery of fines has not been reported for each of these systems and should be a primary metric during pilot scale technology evaluations.

3.4. Precipitation kinetics and modeling

The values of second order kinetic rate constant observed in this study (1.6 – 11.5 h^{-1}) varied with seed loading and initial supersaturation, and were in range and similar to those observed others in both synthetic and real wastewaters. For struvite precipitation, the values of kinetic rate constant vary by more than an order of magnitude in the literature (Table 1). The reason for the large reported range of kinetic rate constant (2.2 – 125 h^{-1}) can likely be attributed to the variations in wastewater aqueous and solid phase compositions. The presence of ionic ligands (calcium, carbonate, organic ligands, etc.) can reduce precipitation rate by forming complexes with magnesium and phosphates and lowering the apparent supersaturation (Moerman, 2011, 2011; Musvoto et al., 2000). The formation of non-struvite minerals (amorphous calcium phosphate (ACP), calcite, magnesium carbonate, dicalcium phosphate dihydrate, etc.) can further also influence struvite production kinetics (Le Corre et al., 2005; Muster et al., 2013). Since the rate of struvite precipitation in anaerobic digestion effluent appears to exhibit an inverse relationship to organic solids concentration, it is possible that sorption of organic contaminants increases the activation energy of secondary crystal growth and heterogeneous nucleation (Table 1). A recent study showed that micro-molar concentrations of alginate, a model polysaccharide, can inhibit crystal growth forming

355 electrostatic bonds with struvite surface functional groups (Wei et al., 2017). This could also
356 stabilize fines, increasing the risk of washout in high rate systems. Future work should focus on
357 the impact of specific impurities on precipitation kinetics and stability of fines.
358
359
360
361 Table 1. Kinetic values of struvite precipitation rate constants available in literature for different
362 wastewater types.

Wastewater type	Struvite precipitation rate constant (h^{-1})
Synthetic (Kazadi Mbamba et al., 2015b)	3.2 ± 1.0
Piggery digestate (Kazadi Mbamba et al., 2015b)	12 ± 10
Sludge digestate (Kazadi Mbamba et al., 2015b)	4.49 ± 1.3
Sludge digestate (Kazadi Mbamba et al., 2015b)[a]	33 ± 13
Anaerobic digester liquor (van Rensburg et al., 2003)	41.7
Anaerobic digested sludge liquor (Musvoto et al., 2000)[b]	12.5
UASB digester supernatant (Musvoto et al., 2000)[b]	125
Postdigestion sludge lagoon supernatant (Ohlinger and Young, 2000)	4.2
Anaerobic swine lagoon liquid (Nelson et al., 2003)[c]	3.7, 7.9, 12.3
This study	1.6 - 11.5

363
364 [a]Sludge digestate: high concentrations of total suspended solids were present (1.1 $kgTSS \cdot m^{-3}$, 4.0 $kgTSS \cdot m^{-3}$, 11.0 $kgTSS \cdot m^{-3}$).
365 [b]Anaerobic digested sludge liquor and UASB digester supernatant: presence and absence of high concentrations of particulate
366 organics inhibited and promoted crystal growth, respectively. [c]Anaerobic swine lagoon liquid: 3.7 h^{-1} at pH 8.4, 7.9 h^{-1} at pH 8.7 and
367 12.3 h^{-1} at pH 9.
368
369
370

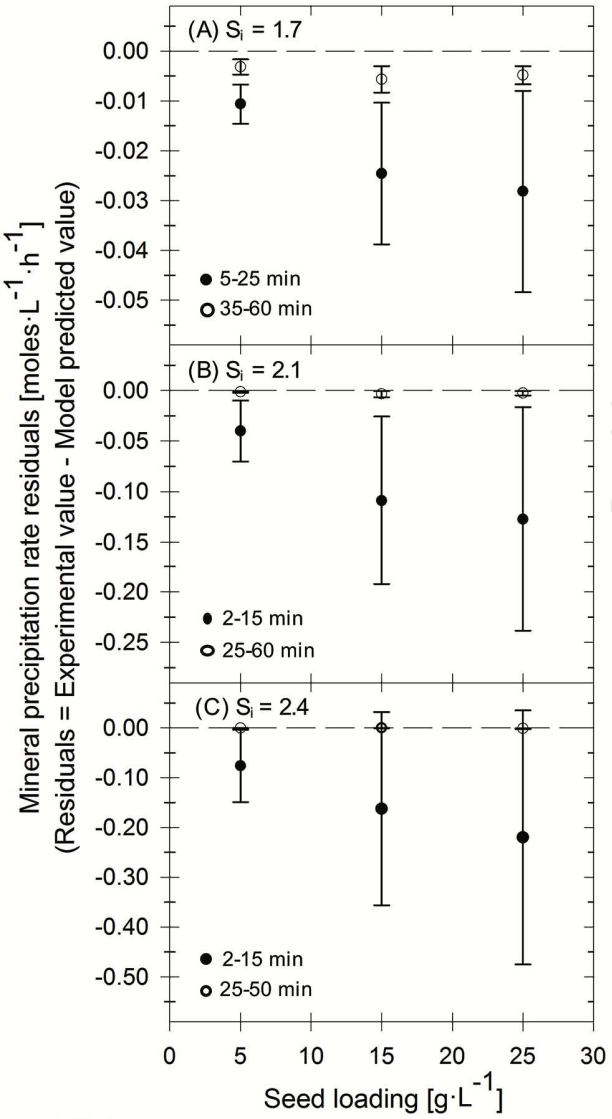

371
372

373 **Fig. 5.** Plots of mineral precipitation rate residuals versus seed loading for different initial supersaturation
374 (S_i) (A) S_i = 1.7 (B) S_i = 2.1 (C) S_i = 2.4 (Residual = Experimental value - Model Predicted Value). Filled
375 circles are the average residuals for the first 3 sampling times and open circles are the residuals for the
376 next 3 sampling points, and error bars represent the standard deviations. Due to faster struvite
377 precipitation at higher S_i, the sampling intervals were reduced from (A) to (C). Complete residuals can be
378 found in Fig. S8 in the SI. Struvite mineral precipitation rate model used was taken from Kazadi Mbamba
379 et al., 2015b, 2015a.

380

Modeling the struvite production with 1st order dependence on seed loading (Eq. 4) will severely over-predict the rate of precipitation at higher seed loadings. Residuals between predicted and observed mineral precipitation rate (Fig. 5, Fig. S8) were significant for all seeded conditions and increased with seed loading. When the mass seed crystals were included in the growth equation, simulated rates of mineral precipitation predict complete removal of the total phosphate (2.2 mM) in all batch experiments within 7.8 mins (at 5 g·L^{-1}, S_i = 1.7) to 0.15 mins (at 25 g·L^{-1}, S_i = 2.4). This is in contradiction to our experimental results in (Fig. 2, Fig. S2) which show only a partial removal of total phosphate across all seed loadings and initial supersaturations after 180 mins. The discrepancy between predicted P removal and experimental data also stems from our observation that the kinetic rate constant for struvite precipitation is not fixed, and exhibits dependence on both seed loading and initial supersaturation. Mineral seed loadings used in our batch experiments were comparatively higher than the experiments used to calibrate and validate Eq. 4 (0.085 g·L^{-1}, 0.1 g·L^{-1}) (Kazadi Mbamba et al., 2015b; Mehta and Batstone, 2013). Our batch experiments were conducted with a seed size of 0.9 mm (sourced from working Ostara Pearl^{TM} reactors) while others have worked with moderately lower seed sizes such as 53-297 µm (Shih et al., 2017), 250 µm (Rahaman et al., 2008) and 30-50 µm (Kazadi Mbamba et al., 2015b; Mehta and Batstone, 2013), which does not reflect the reality of full-scale P recovery processes in which struvite crystals as large as 4.5 mm in size are produced. It is possible that distinguishing between the mass of crystals and fines within a crystallization reactor may improve the predictive capabilities of mass dependent models.

To accurately predict both phosphate removal rate and precipitate recovery, struvite crystallization models must distinguish between the relative abundance of high settling velocity seed crystals and fine crystallites that are difficult to capture. Since fines production may be responsible for the majority of P removal, lumping nucleation or fines kinetics into a crystal growth rate expressions based on seed crystal diameter (Rahaman et al., 2014) will only

accurately predict P removal and growth if: i) secondary growth dictates kinetics, or ii) fines dictate kinetics but agglomeration onto seeds is so rapid that fines are not observed in the system. Efforts have been made to describe precipitation in physio-chemical models using Monod-style mineral rate expressions for different individual pathways of precipitation (Lizarralde et al., 2015). Incorporating switching functions into the expressions of nucleation, crystal growth, agglomeration, and breakage may give more dynamic control over the simultaneous reactions taking place in a system, depending upon which pathway is dominant. However, model development must also consider the constraints of characterizing individual precipitation pathways in the field. In the laboratory, dynamic light scattering, particle counting, and atomic force microscopy can be use understand precipitation pathways, quantify nucleation kinetics, and characterize particle size distributions at the lab-scale, but these techniques will not be available to calibrate a model in the field. A more realistic approach may be to first study kinetics and particle dynamics at lab-scale and use settling column tests and total solids concentration at full-scale to estimate particle size distributions and the balance between secondary crystal growth and fines formation.

4. Conclusions

These results show how variations in seed loading and initial supersaturation conditions can have a significant impact on the rate of phosphate removal, the role of primary versus secondary struvite crystal growth, and the validity of mass dependent kinetic precipitation models. The key findings are as follow:

- Formation of struvite fines was observed in majority of the experiments and found to govern the rate of struvite precipitation;
- P removal kinetics and fines formation exhibited dependence on both seed loading and initial supersaturation.

- The presence of seed granules indirectly increased the rate of struvite precipitation by reducing nucleation induction time;

A key challenge for the design, operation, and modeling of struvite recovery processes will be to understand the dynamics of fine particles in the presence of larger seed crystals and soluble ligands. The pathway towards a consensus struvite precipitation process model must incorporate some form particle size distribution, while also considering the constraints of model calibration and validation at the plant-scale. By understanding the dynamic interactions between secondary growth processes and fines formation, and tuning operational parameters of seed crystal loading and initial supersaturation, kinetic models for struvite precipitation can be better used to optimize reactor design based upon the balance needed between struvite removal and recovery. Understanding the impacts of ionic ligands, organic contaminants, and co-precipitation products in sidestream wastewater on the precipitation kinetics and fines stability will also be critical. In the meantime, accounting for the production and capture of fines must be incorporated into the capital and operating cost estimates of struvite recovery systems.

5. Acknowledgments

The authors thank the generous support of the Department of Civil and Environmental Engineering Kinra research fellowship for supporting S. Agrawal. We would also like to thank Ahren Britton of Ostara for providing the seed material used in this study and Wendell Khundjar for helpful discussions. During the preparation of this manuscript R. D. Cusick and J. S. Guest were supported by NSF Award Number 1739788.

458

459

460 **References:**

461 Abbona, F., Boistelle, R., 1979. Growth morphology and crystal habit of struvite crystals
462 (MgNH4PO4· 6 H2O). J. Cryst. Growth 46, 339–354.
463 Abbona, F., Calleri, M., Ivaldi, G., 1984. Synthetic struvite, MgNH4PO4.6H2O: correct polarity
464 and surface features of some complementary forms. Acta Crystallogr. Sect. B 40, 223–
465 227. https://doi.org/doi:10.1107/S0108768184002020
466 Abbona, F., Madsen, H.L., Boistelle, R., 1982. Crystallization of two magnesium phosphates,
467 struvite and newberyite: effect of pH and concentration. J. Cryst. Growth 57, 6–14.
468 Battistoni, P., Pavan, P., Cecchi, F., Mata-Alvarez, J., 1998. Phosphate removal in real
469 anaerobic supernatants: Modelling and performance of a fluidized bed reactor. Water
470 Sci. Technol., Water Quality International '98 38, 275–283.
471 https://doi.org/10.1016/S0273-1223(98)00412-0
472 Baur, R., Prasad, R., Britton, A., 2008. Reducing Ammonia and Phosphorus Recycle Loads by
473 Struvite Harvesting. Proc. Water Environ. Fed. 2008, 6262–6270.
474 https://doi.org/10.2175/193864708788809671
475 Bhuiyan, M.I.H., Mavinic, D.S., Beckie, R.D., 2008. Nucleation and growth kinetics of struvite in
476 a fluidized bed reactor. J. Cryst. Growth 310, 1187–1194.
477 https://doi.org/10.1016/j.jcrysgro.2007.12.054
478 Bhuiyan, M.I.H., Mavinic, D.S., Beckie, R.D., 2007. A Solubility and Thermodynamic Study of
479 Struvite. Environ. Technol. 28, 1015–1026. https://doi.org/10.1080/09593332808618857
480 Britton, A., Koch, F.A., Mavinic, D.S., Adnan, A., Oldham, W.K., Udala, B., 2005. Pilot-scale
481 struvite recovery from anaerobic digester supernatant at an enhanced biological
482 phosphorus removal wastewater treatment plant. J. Environ. Eng. Sci. 4, 265–277.
483 https://doi.org/10.1139/s04-059
484 Britton, A., Prasad, R., Balzer, B., Cubbage, L., 2009. Pilot testing and economic evaluation of
485 struvite recovery from dewatering centrate at HRSD's Nansemond WWTP, in:
486 Proceedings of the International Conference on Nutrient Recovery from Wastewater
487 Streams. pp. 193–202.
488 Burn, S., Muster, T., Kaksonen, A., Tjandraatmadja, G., 2014. Resource Recovery from
489 Wastewater: A Research Agenda (No. NTRY2C13). Water Environment Research
490 Foundation (WERF), Alexandria, VA.
491 Clark, D., Hunt, G., Kasch, M.S., Lemonds, P.J., Moen, G.M., Neethling, J., 2010. Nutrient
492 Management: Regulatory Approaches to Protect Water Quality. Water Environment
493 Research Foundation.
494 Crutchik, D., Garrido, J.M., 2011. Struvite crystallization versus amorphous magnesium and
495 calcium phosphate precipitation during the treatment of a saline industrial wastewater.
496 Water Sci. Technol. 64, 2460–2467.
497 Crutchik, D., Morales, N., Vázquez-Padín, J.R., Garrido, J.M., 2017. Enhancement of struvite
498 pellets crystallization in a full-scale plant using an industrial grade magnesium product.
499 Water Sci. Technol. 75, 609–618. https://doi.org/10.2166/wst.2016.527
500 Desmidt, E., Ghyselbrecht, K., Zhang, Y., Pinoy, L., Bruggen, B.V. der, Verstraete, W., Rabaey,
501 K., Meesschaert, B., 2015. Global Phosphorus Scarcity and Full-Scale P-Recovery
502 Techniques: A Review. Crit. Rev. Environ. Sci. Technol. 45, 336–384.
503 https://doi.org/10.1080/10643389.2013.866531

Galbraith, S.C., Schneider, P.A., Flood, A.E., 2014. Model-driven experimental evaluation of struvite nucleation, growth and aggregation kinetics. Water Res. 56, 122–132. https://doi.org/10.1016/j.watres.2014.03.002

Grooms, A., Reusser, S., Dose, A., Britton, A., Prasad, R., 2015. Operating Experience with Ostara Struvite Harvesting Process. Proc. Water Environ. Fed. 2015, 2162–2177. https://doi.org/10.2175/193864715819538651

Jaffer, Y., Clark, T.A., Pearce, P., Parsons, S.A., 2002. Potential phosphorus recovery by struvite formation. Water Res. 36, 1834–1842. https://doi.org/10.1016/S0043-1354(01)00391-8

Kazadi Mbamba, C., Batstone, D.J., Flores-Alsina, X., Tait, S., 2015a. A generalised chemical precipitation modelling approach in wastewater treatment applied to calcite. Water Res. 68, 342–353. https://doi.org/10.1016/j.watres.2014.10.011

Kazadi Mbamba, C., Flores-Alsina, X., John Batstone, D., Tait, S., 2016. Validation of a plant-wide phosphorus modelling approach with minerals precipitation in a full-scale WWTP. Water Res. 100, 169–183. https://doi.org/10.1016/j.watres.2016.05.003

Kazadi Mbamba, C., Tait, S., Flores-Alsina, X., Batstone, D.J., 2015b. A systematic study of multiple minerals precipitation modelling in wastewater treatment. Water Res. 85, 359–370. https://doi.org/10.1016/j.watres.2015.08.041

Kofina, A.N., Koutsoukos, P.G., 2005. Spontaneous Precipitation of Struvite from Synthetic Wastewater Solutions. Cryst. Growth Des. 5, 489–496. https://doi.org/10.1021/cg049803e

Latimer, R., Rohrbacher, J., Nguyen, V., Khunjar, W.O., Jenyananyagam, S., Alexander, R., Mehta, C., Batstone, D., 2016. Towards a Renewable Future: Assessing Resource Recovery as a Viable Treatment Alternative State of the Science and Market Assessment. IWA Publishing.

Le Corre, K.S., Valsami-Jones, E., Hobbs, P., Parsons, S.A., 2005. Impact of calcium on struvite crystal size, shape and purity. J. Cryst. Growth 283, 514–522. https://doi.org/10.1016/j.jcrysgro.2005.06.012

Lizarralde, I., Fernández-Arévalo, T., Brouckaert, C., Vanrolleghem, P., Ikumi, D.S., Ekama, G.A., Ayesa, E., Grau, P., 2015. A new general methodology for incorporating physico-chemical transformations into multi-phase wastewater treatment process models. Water Res. 74, 239–256. https://doi.org/10.1016/j.watres.2015.01.031

Mehta, C.M., Batstone, D.J., 2013. Nucleation and growth kinetics of struvite crystallization. Water Res. 47, 2890–2900. https://doi.org/10.1016/j.watres.2013.03.007

Mihelcic, J.R., Fry, L.M., Shaw, R., 2011. Global potential of phosphorus recovery from human urine and feces. Chemosphere, The Phosphorus Cycle 84, 832–839. https://doi.org/10.1016/j.chemosphere.2011.02.046

Moerman, W.H.M., 2011. Full Scale Phosphate Recovery: Process Control Affecting Pellet Growth and Struvite Purity. Proc. Water Environ. Fed. 2011, 866–878.

Münch, E.V., Barr, K., 2001. Controlled struvite crystallisation for removing phosphorus from anaerobic digester sidestreams. Water Res. 35, 151–159. https://doi.org/10.1016/S0043-1354(00)00236-0

Muster, T.H., Douglas, G.B., Sherman, N., Seeber, A., Wright, N., Güzükara, Y., 2013. Towards effective phosphorus recycling from wastewater: Quantity and quality. Chemosphere 91, 676–684. https://doi.org/10.1016/j.chemosphere.2013.01.057

Musvoto, E.V., Wentzel, M.C., Ekama, G.A., 2000. Integrated chemical–physical processes modelling—II. simulating aeration treatment of anaerobic digester supernatants. Water Res. 34, 1868–1880. https://doi.org/10.1016/S0043-1354(99)00335-8

Nelson, N.O., Mikkelsen, R.L., Hesterberg, D.L., 2003. Struvite precipitation in anaerobic swine lagoon liquid: effect of pH and Mg:P ratio and determination of rate constant. Bioresour. Technol. 89, 229–236. https://doi.org/10.1016/S0960-8524(03)00076-2

555 Ohlinger, K.N., Young, T.M., 2000. Postdigestion Struvite Precipitation Using a Fluidized Bed
556 Reactor. J. Environ. Eng. 126, 361.
557 Ohlinger, K.N., Young, T.M., Schroeder, E.D., 1999. Kinetics effects on preferential struvite
558 accumulation in wastewater. J. Environ. Eng. 125, 730–737.
559 Ohlinger, K.N., Young, T.M., Schroeder, E.D., 1998. Predicting struvite formation in digestion.
560 Water Res. 32, 3607–3614. https://doi.org/10.1016/S0043-1354(98)00123-7
561 Parsons, S.A., Smith, J.A., 2008. Phosphorus Removal and Recovery from Municipal
562 Wastewaters. Elements 4, 109–112. https://doi.org/10.2113/GSELEMENTS.4.2.109
563 Rahaman, M.S., Mavinic, D.S., Bhuiyan, M.I.H., Koch, F.A., 2006. Exploring the determination
564 of struvite solubility product from analytical results. Environ. Technol. 27, 951–961.
565 Rahaman, M.S., Mavinic, D.S., Ellis, N., 2008. Phosphorus recovery from anaerobic digester
566 supernatant by struvite crystallization: model-based evaluation of a fluidized bed reactor.
567 Water Sci. Technol. 58, 1321–1327. https://doi.org/10.2166/wst.2008.721
568 Rahaman, M.S., Mavinic, D.S., Meikleham, A., Ellis, N., 2014. Modeling phosphorus removal
569 and recovery from anaerobic digester supernatant through struvite crystallization in a
570 fluidized bed reactor. Water Res. 51, 1–10. https://doi.org/10.1016/j.watres.2013.11.048
571 Seckler, M.M., Bruinsma, O.S.L., Van Rosmalen, G.M., 1996. Calcium phosphate precipitation
572 in a fluidized bed in relation to process conditions: A black box approach. Water Res. 30,
573 1677–1685. https://doi.org/10.1016/0043-1354(96)00043-7
574 Shih, Y.-J., Abarca, R.R.M., de Luna, M.D.G., Huang, Y.-H., Lu, M.-C., 2017. Recovery of
575 phosphorus from synthetic wastewaters by struvite crystallization in a fluidized-bed
576 reactor: Effects of pH, phosphate concentration and coexisting ions. Chemosphere 173,
577 466–473. https://doi.org/10.1016/j.chemosphere.2017.01.088
578 Solon, K., Flores-Alsina, X., Kazadi Mbamba, C., Ikumi, D., Volcke, E.I.P., Vaneeckhaute, C.,
579 Ekama, G., Vanrolleghem, P.A., Batstone, D.J., Gernaey, K.V., Jeppsson, U., 2017.
580 Plant-wide modelling of phosphorus transformations in wastewater treatment systems:
581 Impacts of control and operational strategies. Water Res. 113, 97–110.
582 https://doi.org/10.1016/j.watres.2017.02.007
583 Triger, A., Pic, J.-S., Cabassud, C., 2012. Determination of struvite crystallization mechanisms
584 in urine using turbidity measurement. Water Res. 46, 6084–6094.
585 https://doi.org/10.1016/j.watres.2012.08.030
586 US EPA, O., 2016. State Progress Toward Developing Numeric Nutrient Water Quality Criteria
587 for Nitrogen and Phosphorus [WWW Document]. US EPA. URL
588 https://www.epa.gov/nutrient-policy-data/state-progress-toward-developing-numeric-
589 nutrient-water-quality-criteria (accessed 8.26.17).
590 van Rensburg, P., Musvoto, E.V., Wentzel, M.C., Ekama, G.A., 2003. Modelling multiple mineral
591 precipitation in anaerobic digester liquor. Water Res. 37, 3087–3097.
592 https://doi.org/10.1016/S0043-1354(03)00173-8
593 Wang, J., Burken, J., Zhang, X., Surampalli, R., 2005. Engineered Struvite Precipitation:
594 Impacts of Component-Ion Molar Ratios and pH. J. Environ. Eng. 131, 1433–1440.
595 https://doi.org/10.1061/(ASCE)0733-9372(2005)131:10(1433)
596 Wei, L., Hong, T., Liu, H., Chen, T., 2017. The effect of sodium alginate on struvite
597 crystallization in aqueous solution: A kinetics study. J. Cryst. Growth 473, 60–65.
598 https://doi.org/10.1016/j.jcrysgro.2017.03.039
599 Woods, N.C., Sock, S.M., Daigger, G.T., 1999. Phosphorus Recovery Technology Modeling and
600 Feasibility Evaluation for Municipal Wastewater Treatment Plants. Environ. Technol. 20,
601 663–679. https://doi.org/10.1080/09593332008616862
602 Ye, Y., Ngo, H.H., Guo, W., Liu, Y., Li, J., Liu, Y., Zhang, X., Jia, H., 2017. Insight into chemical
603 phosphate recovery from municipal wastewater. Sci. Total Environ. 576, 159–171.
604 https://doi.org/10.1016/j.scitotenv.2016.10.078
605

Highlights

- P removal kinetics and struvite crystal growth were explored in seeded solutions.
- Struvite fines were majority of solids formed under explored conditions.
- Precipitation rate was dependent on initial supersaturation and seed loading.
- Higher seed loading and lower initial supersaturation minimized fines production.
- Struvite process models with linear dependence on seed mass over-predict P removal.